




Cite this: *RSC Adv.*, 2017, 7, 33335

Received 31st May 2017
 Accepted 26th June 2017

DOI: 10.1039/c7ra06080g
rsc.li/rsc-advances

Polyoxometalate-MgF₂ hybrids as heterogeneous solid acid catalysts for efficient biodiesel production†

Kai-Li Yang, Shan Huang, Hu Pan, Heng Zhang, Xiao-Fang Liu and Song Yang *

A series of highly active and stable Keggin heteropolyacid catalysts were prepared through mixing of 12-tungstophosphoric acid (TPA) with magnesium fluoride (MgF₂). Among those acidic catalysts, the Mg₂₀F₃₉TPA-1.0 hybrid with moderate acidity (0.96 mmol g⁻¹) and good dispersion of active sites presented pronounced catalytic performance in esterification of oleic acid (up to 95% oleic acid conversion). Particularly, Mg₂₀F₃₉TPA-1.0 was also efficient for the transesterification of Jatropha oil with a high acid value, giving biodiesel in 93% yield. Moreover, the catalyst showed good durability and reusability for at least five consecutive cycles.

1. Introduction

In the wake of the consumption of fossil fuels and the concomitant aggravation of environmental concerns, there is currently an urgent need to search for renewable and clean energy sources.^{1–3} Due to the merits of biodegradability, non-sulfur, renewability, and high lubricity, biodiesel is considered to be one of promising alternative fuels.^{4–6} Biodiesel is composed of long chain fatty acid monoesters, which are generally derived from renewable oils or fats by (trans)esterification with short carbon-chain alcohols.^{7–9} In the process of producing biodiesel, cheaper oils (*e.g.*, Jatropha oil) have been elected as raw materials to cut the production cost.^{10,11} However, the use of an alkaline catalyst may lead to saponification, difficult separation of products, and high catalyst consumption.^{12–15} In addition, abundant free fatty acids (FFAs) can be generated as important byproducts during food processing.¹⁶ Therefore, it is a beneficial route to use acidic catalysts to esterify FFAs and (trans)esterify Jatropha oil for biodiesel production.

Traditionally, homogeneous acid catalysts (*e.g.*, H₂SO₄, HCl or H₃PO₄) are applied for transesterification and esterification.¹⁷ However, these types of catalytic systems not only need extra neutralization, are energy-intensive and require complicated purification steps, but they are also difficult to recover and

separate, which may increase the cost of biodiesel production.^{18,19}

Therefore, the design and use of solid acid catalysts for either transesterification or esterification have been widely developed to overcome these drawbacks. For example, an ionic liquid functionalized polymer (*e.g.*, poly([VSIM][HSO₄])) exhibited good catalytic activity in oleic acid esterification, giving biodiesel in a conversion of 92%.²⁰ Sulfated zirconia possessing Brønsted and Lewis acid sites afforded 88% biodiesel yield in esterification of stearic acid, while the loss of the Brønsted acid sites directly resulted in significant deactivation of the catalyst.²¹ Sulfonic acid-functionalized solid acids (*e.g.*, sulphonated carbon and SO₃H-SBA-15) were also explored to be used for producing biodiesel from plant oils or fatty acids, giving 82–92% yield of biodiesel at high temperatures (*e.g.*, 200 °C).^{22,23} However, wide application of those materials in biodiesel production was restricted possibly due to their low thermal stability, need of costly raw materials, and rigorous and complicated preparation procedures.

Heteropolyacids (HPAs) have stronger Brønsted acidity than most of mineral acids.^{24–27} However, low surface areas (<10 m² g⁻¹) of HPAs greatly reduce the dispersion and accessibility of acid sites to substrates during reactions, and they are difficult to recover in polar solvents because of high miscibility.²⁸ To address these issues, HPAs were usually immobilized onto porous materials (*e.g.*, HPMo/A20 and TPA/ZrO₂),^{29,30} while the problem of leaching remained heavily in the production of biodiesel. Instead, solvothermal method seems to be a valid solution to overcome this drawback, with active sites dispersed more evenly.^{31,32} The solidification with cations is another way to overcome the solubility of HPAs. However, a comparison of immobilization and solidification methods showed that the latter possessed higher density of acidic sites and better catalytic performance.^{33,34}

State Key Laboratory Breeding Base of Green Pesticide & Agricultural Bioengineering, Key Laboratory of Green Pesticide & Agricultural Bioengineering, Ministry of Education, State-Local Joint Laboratory for Comprehensive Utilization of Biomass, Center for Research & Development of Fine Chemicals, Guizhou University, Guiyang 550025, China. E-mail: jhxx.msm@gmail.com; Fax: +86 851 88292170; Tel: +86 851 88292171

† Electronic supplementary information (ESI) available. See DOI: 10.1039/c7ra06080g



It was reported that MgF_2 possessed high thermal stability, mesoporous structure, Brønsted and Lewis acid sites.³⁵ Besides, it also contains moderate weak base sites (0.65 mmol g^{-1}). Therefore, MgF_2 can be a promising support to solidify TPA, without destructing the structure of TPA. Herein, a series of polyoxometalate- MgF_2 ($\text{Mg}_{20}\text{F}_{39}\text{TPA-x}$) were synthesized from mixing of TPA with MgF_2 . For the sake of evaluating the catalytic performance of $\text{Mg}_{20}\text{F}_{39}\text{TPA-x}$, the catalysts were used for producing biodiesel from both oleic acid and Jatropha oil with a high acid value of 19.35 mg KOH/g *via* esterification and transesterification, respectively.

2. Experimental

2.1 Materials

Mg (99.9%) and HF (49 wt% in water, 99.99998%) were bought from Aladdin Industrial Inc. (Shanghai). Methanol (>99.5%) was supplied by Guanghua scientific Ltd. (Guangdong). $\text{H}_3\text{-PW}_{12}\text{O}_{40}\cdot n\text{H}_2\text{O}$ (AR) and Oleic acid (AR) were purchased from Kemiou Chemical Reagent, Co., Ltd. (Tianjin). Jatropha oil ($\geq 98\%$, Table 1) procured from Luodian County, Guizhou Province, China.

2.2 Catalyst preparation

2.2.1 Synthesis of MgF_2 . The MgF_2 catalysts were synthesized *via* a sol-gel method.³⁵ In a typical procedure, excessive methanol (30 mL) was first added into metallic magnesium (0.39 g, 16 mmol) at room temperature. After magnesium was dissolved completely, HF (32 mmol) was added under stirring conditions, and the resulting mixtures were stirred for 24 h. The sols could form viscous transparent gels as they were aged for 24 h at room temperature. Then drying of this gels were accomplished at 80°C for 24 h, and the dried powders were calcined at 200°C for 3 h with a heating rate of 2°C min^{-1} in furnace.

2.2.2 Synthesis of 30 wt% TPA/ MgF_2 . The 30 wt% TPA/ MgF_2 was synthesized by incipient wetness impregnation method. After TPA (30 wt%) was dissolved completely in methanol, MgF_2 was added under stirring conditions. The resulting mixtures were stirred for 30 min, and aged at 40°C for 24 h, which was further dried at 80°C overnight. Finally, the white powder was calcined at 200°C for 3 h with a heating rate of 2°C min^{-1} in furnace.

2.2.3 Synthesis of $\text{Mg}_{20}\text{F}_{39}\text{TPA-x}$. To a solution of metallic magnesium (0.49 g, 20 mmol) dissolved in methanol (40 mL) at room temperature, HF (39 mmol) and $\text{H}_3\text{PW}_{12}\text{O}_{40}\cdot n\text{H}_2\text{O}$ (1.2 mmol, 1.0 mmol, 0.8 mmol, or 0.6 mmol) in methanol (10 mL) were added into the former solution at room temperature. Some white precipitates were formed, and the resulting

suspension was stirred for 24 h, and aged at 40°C for 24 h, which was further transferred to an autoclave and solvothermally treated at 200°C for 2 h with a heating rate of 2°C min^{-1} . Subsequently, the suspension was dried at 40°C for 24 h and further dried at 80°C overnight. Finally, the white powder was calcined at 200°C for 3 h with a heating rate of 2°C min^{-1} in furnace. The prepared catalysts were named as $\text{Mg}_{20}\text{F}_{39}\text{TPA-x}$ (where x is the content of TPA; $x = 1.2, 1.0, 0.8, \text{ and } 0.6 \text{ mmol}$) that represents $\text{Mg}_{20}\text{F}_{39}\text{-H}_{2.6}\text{P}_{1.2}\text{W}_{14.4}\text{O}_{48}$, $\text{Mg}_{20}\text{F}_{39}\text{H}_{2.0}\text{PW}_{12}\text{O}_{40}$, $\text{Mg}_{20}\text{F}_{39}\text{H}_{1.4}\text{P}_{0.8}\text{W}_{9.6}\text{O}_{32}$, and $\text{Mg}_{20}\text{F}_{39}\text{H}_{0.8}\text{P}_{0.6}\text{W}_{9.6}\text{O}_{32}$, respectively.

2.3 Catalyst characterization

Fourier transform-infrared (FT-IR) spectra of samples were recorded on a Nicolet 360 FT-IR spectrometer by using a KBr disc method. Energy dispersive X-ray spectroscopy (EDS; S-4800, Hitachi) under 5 kV primary electron voltages was employed to measure the elemental components. X-ray diffraction (XRD) patterns in the 2θ angle from 5 to 80° were obtained on D8 ADVANCE X-ray diffractometer (Cu $K\alpha$ radiation, $\lambda = 0.154 \text{ nm}$). The surface properties were determined by nitrogen adsorption-desorption over Micromeritics ASAP 2020 M analyzer at -196°C . The surface areas, pore-volumes and pore-size distributions were calculated by Brunauer-Emmett-Teller (BET) method and Barrett-Joyner-Halenda (BJH) method, respectively. Transmission electron microscopy (TEM) observations were achieved on a HT7700 system operated at 200 kV. Thermogravimetric (TG) test was conducted on a METTLER TGA/DSC1 apparatus in nitrogen atmosphere with heating rate of $10^\circ\text{C min}^{-1}$. According to the curves of ammonia/carbon dioxide temperature-programmed desorption ($\text{NH}_3/\text{CO}_2\text{-TPD}$), the content of acid sites were measured and calculated on AutoChem 2920 chemisorption analyzer. Approximately 0.1 g catalyst was pretreated under He flow (30 mL min^{-1}) at 300°C for 2 h, then saturated with ammonia by exposing to $10\% \text{ NH}_3\text{-He}$ or $10\% \text{ CO}_2\text{-He}$ at 50°C . The physically adsorbed ammonia was flushed with He. The desorbed ammonia was recorded under a temperature rate of $10^\circ\text{C min}^{-1}$ until heated up to $500\text{--}700^\circ\text{C}$. Elemental analyzer (Vario EL III) was used to measure the carbon contents of the catalysts.

2.4 Catalytic test

2.4.1 Esterification of oleic acid. The reaction of esterification was conducted in a 25 mL sealed autoclave and heated in an oil bath. In a general procedure, the Teflon-lined stainless-steel autoclave with catalyst (3–7 wt%), oleic acid (2 g), and dried methanol (methanol/oleic acid molar ratio = 6/1–18/1) was placed into the oil bath at a previously set temperature ($50\text{--}90^\circ\text{C}$, 600 rpm). The temperature was controlled by temperature-sensor with an accuracy of 1°C . After reaction (1–5

Table 1 The fatty acid composition of Jatropha oil

Fatty acid	Palmitic acid (C16:0)	Palmitoleic acid (C16:1)	Stearic acid (C18:0)	Oleic acid (C18:1)	Linoleic acid (C18:2)	Linolenic acid (C18:3)
Content (wt%)	13.23	0.85	5.40	41.62	36.99	0.22



h), the mixture was cooled by using water bath. The solid catalyst was separated by centrifugation, washed several times with *n*-hexane, dried at 80 °C, and further used for the next reaction. The upper layer was rotarily evaporated at 80 °C to eliminate methanol and water.

The conversion of oleic acid was determined *via* a titration method by employing 0.1 M standard potassium hydroxide ethanol solution as titrant and phenolphthalein as indicator. It was calculated depending on the below equation:

$$\text{Oleic acid conversion (\%)} = (1 - AV_0/AV_1) \times 100\%$$

where AV_0 represents initial acid value of oleic acid, AV_1 represents final acid value after esterification.

2.4.2 Simultaneous esterification and transesterification of Jatropha oil. The Teflon-lined stainless-steel autoclave containing catalyst (10 wt%), Jatropha oil (19.35 mg KOH/g, 2 g), and dried methanol (1.4 g based on methanol/oil molar ratio of 20/1) was placed into an oil bath preheated to a set temperature under stirring (130 °C, 600 rpm). The mixture was cooled in water bath after reacting for 10 h and separated by centrifugation. Then the upper layer was rotarily evaporated at 80 °C, and tested by gas chromatograph (GC; Agilent 7890B) with capillary column of HP-5 (30 m × 0.320 mm × 0.25 mm) and flame ionization detector (FID).³⁶ The oven program temperature was set from 180 °C to 240 °C under a heating rate of 15 °C min⁻¹. Meanwhile, the initial and final temperature was kept for 2 min and 8 min, respectively. The injector and detector temperatures were 250 °C. The flow rate of carrier gas (N₂), air and H₂ were 45 mL min⁻¹, 450 mL min⁻¹, and 40 mL min⁻¹, respectively. The split ratio was 20/1, and the injection volume was 1 μL. Heptadecanoic acid methyl ester was employed as internal standard.

According to the weights and GC peak areas of crude biodiesel and heptadecanoic acid methyl ester, biodiesel yield was calculated by following equation:

$$\text{Yield (wt\%)} = \left\{ \frac{A_{C16:0}f_{C16:0} + A_{C16:1}f_{C16:1} + A_{C18:0}f_{C18:0} + A_{C18:1}f_{C18:1} + A_{C18:2}f_{C18:2} + A_{C18:3}f_{C18:3} + A_{C_{\text{others}}}A_{C17:0}}{\text{weight of } C_{17:0}} \right\} / (\text{weight of crude biodiesel}) \times 100\%$$

where f_{Cn} (the relative response factor) is 1.014, 1.023, 1.076, 1.038, 1.019 and 0.926 ($n = 16:0, 16:1, 18:0, 18:1, 18:2, 18:3$), respectively; A represents the GC peak area of Cn , other components and $C_{17:0}$ (heptadecanoic acid methyl ester). Three repeated experiments have been conducted for each experiment, and the results are shown in average value with standard deviation (σ) of 0.6–2.3%.

3. Results and discussion

3.1 Catalysts characterization

In order to demonstrate that the TPA was not in a crystalline state but molecularly dispersed on the surface of magnesium fluoride material, XRD patterns of Mg₂₀F₃₉TPA-1.0, bare TPA and MgF₂ were conducted (Fig. 1). TPA (curve c) exhibited a series of sharp characteristic diffraction peaks of Keggin ion at

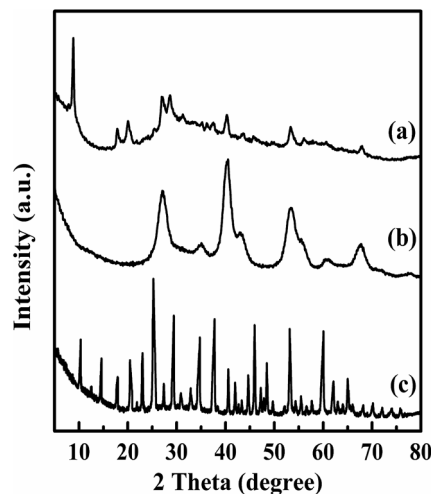


Fig. 1 XRD patterns of (a) Mg₂₀F₃₉TPA-1.0, (b) MgF₂, and (c) TPA.

10.23°, 17.78°, 20.43°, 25.09°, 29.42° and 37.66°, respectively.³⁷ The catalysts all (curve a, curve b) displayed the typical reflections of MgF₂ at 27.14°, 40.41°, 53.21° and 67.62°.³⁵ And the resultant Mg₂₀F₃₉TPA-1.0 catalyst (curve a) also showed the characteristic diffraction peaks of Keggin ion at 8.86°, 17.98°, 20.29° and 28.51°. Even though characteristic peaks of Mg₂₀F₃₉TPA-1.0 are very similar to Keggin ion of TPA and MgF₂, the slight shift were happened, especially at 10.23°, indicating that the metal salt was formed for the exchange of protons with metal ions.³⁸ Besides, the peaks widths of Mg₂₀F₃₉TPA-1.0 broadened and the intensity of peaks decreased, demonstrating that the chemical interactions was occurred between TPA and Mg₂₀F₃₉, and the TPA was semidispersed on catalyst.³⁹

EDS analysis results were obtained by EDS measurement: Mg, 12.65, W, 9.08 (Mg₂₀F₃₉TPA-1.2); Mg, 12.41 and W, 7.63 (Mg₂₀F₃₉TPA-1.0); Mg, 13.08, W, 6.47 (Mg₂₀F₃₉TPA-0.8); Mg, 15.68 and W, 4.91 (Mg₂₀F₃₉TPA-0.6). The W/Mg atomic ratios of Mg₂₀F₃₉TPA- x were described in Table 2, and the results were consistent with the theoretical values, indicating that there was no sole TPA in Mg₂₀F₃₉TPA- x . From the EDS spectra of Mg₂₀F₃₉TPA- x catalysts in Fig. S1(b–e),[†] extra characteristic peaks of P and W elements were appeared, which were not presented on the spectrum of MgF₂ (Fig. S1(a)[†]), suggesting that the Mg₂₀F₃₉TPA- x hybrids were formed.⁴⁰ These results were in good agreement with those of XRD patterns.

Table 2 EDS analysis for Mg₂₀F₃₉TPA- x ($x = 1.2, 1.0, 0.8, 0.6$)^a

Catalyst	W/Mg nominal ratio	W/Mg average value from EDS
Mg ₂₀ F ₃₉ TPA-1.2	0.72	0.72
Mg ₂₀ F ₃₉ TPA-1.0	0.60	0.61
Mg ₂₀ F ₃₉ TPA-0.8	0.48	0.49
Mg ₂₀ F ₃₉ TPA-0.6	0.36	0.31

^a Mg₂₀F₃₉TPA- x denoted as Mg₂₀F₃₉H_{2.6}P_{1.2}W_{14.4}O₄₈, Mg₂₀F₃₉H_{2.0}PW₁₂O₄₀, Mg₂₀F₃₉H_{1.4}P_{0.8}W_{9.6}O₃₂, and Mg₂₀F₃₉H_{0.8}P_{0.6}W_{9.6}O₃₂.



FT-IR spectra of $\text{Mg}_{20}\text{F}_{39}\text{TPA-1.0}$ and TPA were exhibited in Fig. 2. Four featured peaks of TPA Keggin ion could be observed at 1080, 980, 893 and 800 cm^{-1} , which might be attributed to P–O_a, W = O_d, W–O_b–W and W–O_c–W, respectively.³² The FT-IR spectra of other $\text{Mg}_{20}\text{F}_{39}\text{TPA-}x$ catalysts ($x = 1.2, 0.8, \text{ and } 0.6$) were provided in Fig. S2.† Keggin structure of all $\text{Mg}_{20}\text{F}_{39}\text{TPA-}x$ catalysts was found to remain unchanged, despite slight weakening in some peak strengths, which could be ascribed to the decrease of the TPA ratio in $\text{Mg}_{20}\text{F}_{39}\text{TPA-}x$.⁴¹

The acidity of $\text{Mg}_{20}\text{F}_{39}\text{TPA-}x$ was determined by NH_3 -TPD, and the results were listed in Table 3. As expected, the increase of proton number in $\text{Mg}_{20}\text{F}_{39}\text{TPA-}x$, obtained by the increase of the TPA contents led to the rise of acidity of the solid. As shown in Fig. S3,† TPA was characterized by weak and strong acidic sites, and MgF_2 showed weak and moderate acidic sites as evidenced from TPD determination. Correspondingly, NH_3 -TPD curves of $\text{Mg}_{20}\text{F}_{39}\text{TPA-}x$ displayed the weak, moderate and strong acidic sites located at 100–300 °C, 300–500 °C and 500–700 °C. In this respect, it could be explained that the moderate acidic sites were mainly from the $\text{Mg}_{20}\text{F}_{39}$ moiety.⁴² In Fig. S5,† the pore size and surface area of $\text{Mg}_{20}\text{F}_{39}\text{TPA-1.0}$ was found to be 5.4 nm and 25.4 $\text{m}^2 \text{g}^{-1}$, respectively. Nitrogen adsorption–desorption experiment displayed that the mesoporous structure was formed in $\text{Mg}_{20}\text{F}_{39}\text{TPA-1.0}$, which is beneficial to mass transfer during the transesterification and esterification. Although the surface area

of $\text{Mg}_{20}\text{F}_{39}\text{TPA-1.0}$ was small, the narrow pore size distribution was observed, which was mainly centered at 4–6 nm. It was indicated that the pores were distributed in the surface of $\text{Mg}_{20}\text{F}_{39}\text{TPA-1.0}$ are uniform. As shown in Fig. S4,† the weak basicity (0.65 mmol g^{-1}) of MgF_2 could be measured. As expected, it is advantageous to form polyoxometalate- MgF_2 hybrids without destroying the structure of TPA due to the weak basicity of MgF_2 . This fact verified the results of XRD and FT-IR.

The dispersion of $\text{Mg}_{29}\text{F}_{30}\text{TPA-1.0}$ particles was analyzed by TEM (Fig. 3), and a large number of worm-like mesoporous structure could be observed. These nanoparticles in small size of 2–7 nm were clearly observed. This result is in good agreement with nitrogen adsorption–desorption analysis of $\text{Mg}_{29}\text{F}_{30}\text{TPA-1.0}$ that shows uniform mesoporous structure with average pore size of 5.3 nm.

Fig. S6† exhibits the thermal stability of $\text{Mg}_{20}\text{F}_{39}\text{TPA-1.0}$ catalyst studied by TG analyses. It can be seen that $\text{Mg}_{20}\text{F}_{39}\text{TPA-1.0}$ has an excellent thermal stability with less weight loss (about 5 wt%) at 100–350 °C, which is possibly attributed to desorption of water molecules inside the catalyst pores. Thus, it has great potential to be used at high reaction temperatures.

3.2 The comparison of catalytic activities

The catalytic activities of different catalyst were tested for oleic acid esterification. In the reaction, the relatively low methanol/oleic acid molar ratio of 9 : 1 was employed at 80 °C with 5 wt% catalyst dosage for 4 h, and the results were displayed in Fig. 4. The conversion of oleic acid reached to 10% without any catalyst under the above reaction conditions, indicating that the catalytic activity was attributed to the weak acidity of oleic acid, wherein it might act as both catalyst and reactant.⁴³ Sole MgF_2 presented conversion of 15%. The slight increase of conversion during esterification could be resulted from the existence of Brønsted and Lewis acid sites in MgF_2 . Although the conversion over TPA was 94% in oleic acid conversion, the catalyst was soluble in this reaction system, which made it difficult to reuse. Gratifyingly, excellent conversions were also gained when the esterification was performed in the presence of $\text{Mg}_{20}\text{F}_{39}\text{TPA-}x$ catalysts. From Fig. 4, the sequence of catalytic activities for these TPA salt catalysts was $\text{Mg}_{20}\text{F}_{39}\text{TPA-1.2} \sim \text{Mg}_{20}\text{F}_{39}\text{TPA-1.0} > \text{Mg}_{20}\text{F}_{39}\text{TPA-0.8} > \text{Mg}_{20}\text{F}_{39}\text{TPA-0.6}$, according to the oleic acid conversion. It is obviously to see that the total acidity of the catalysts directly influenced their catalytic activity, which is in accordance with the proposal that Brønsted acid take main

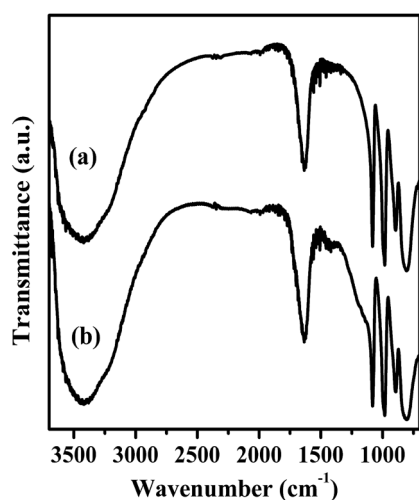


Fig. 2 FTIR spectra of (a) TPA and (b) $\text{Mg}_{20}\text{F}_{39}\text{TPA-1.0}$.

Table 3 Acidity of $\text{Mg}_{20}\text{F}_{39}\text{TPA-}x$ catalysts

Catalysts	Acidity (mmol g^{-1})				Molar ratio		
	Weak (100–300 °C)	Moderate (300–500 °C)	Strong (500–700 °C)	Total	W/T^a	M/T^a	S/T^a
$\text{Mg}_{20}\text{F}_{39}\text{TPA-1.2}$	0.35	0.23	0.43	1.01	0.35	0.23	0.43
$\text{Mg}_{20}\text{F}_{39}\text{TPA-1.0}$	0.30	0.26	0.40	0.96	0.31	0.27	0.42
$\text{Mg}_{20}\text{F}_{39}\text{TPA-0.8}$	0.50	0.13	0.30	0.93	0.54	0.14	0.32
$\text{Mg}_{20}\text{F}_{39}\text{TPA-0.6}$	0.49	0.08	0.06	0.63	0.78	0.13	0.09

^a W = density of weak acid sites, M = density of moderate acid sites, S = density of strong acid sites, and T = density of total acid sites.



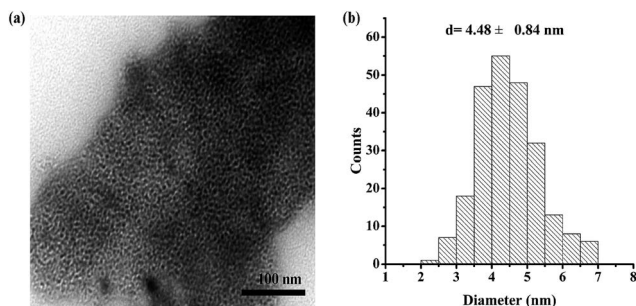


Fig. 3 (a) TEM image, (b) particle size distribution of $\text{Mg}_{29}\text{F}_{39}\text{TPA-1.0}$.

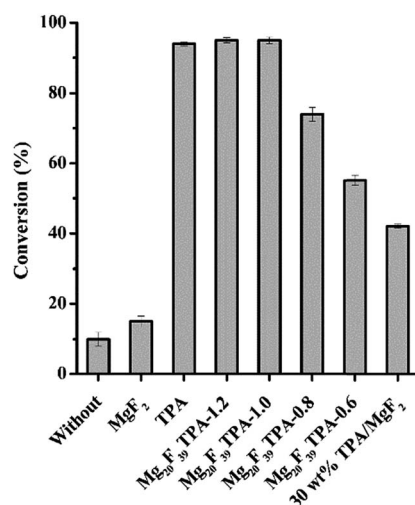


Fig. 4 Catalytic performance of different catalysts in the conversion of oleic acid to methyl oleate. Reaction conditions: methanol/oleic acid molar ratio = 9/1, catalyst dosage = 5 wt%, reaction time = 4 h, and reaction temperature = 80 °C.

effect in esterification.⁴⁴ In addition, the conversion of oleic acid was increased significantly from 74% to 95% with the protons of TPA rose from 1.4 to 2.0. It was worth noticing that the total acidity of $\text{Mg}_{20}\text{F}_{39}\text{TPA-x}$ increased slightly (0.93–0.96 mmol g^{-1}), however, the density of strong acid sites was raised obviously from 0.30 to 0.40 mmol g^{-1} . Further increasing of protons of TPA from 2.0 to 2.4 resulting slightly enhanced strong acid sites (0.40 to 0.43 mmol g^{-1}) with a conversion of 95%, which is identical to that of over $\text{Mg}_{20}\text{F}_{39}\text{TPA-1.0}$. On the other hand, the acidity of 30 wt% TPA/ MgF_2 prepared by impregnation method was demonstrated to be 0.41 mmol g^{-1} (Fig. S3†), which was far less than that of $\text{Mg}_{20}\text{F}_{39}\text{TPA-x}$ (0.63–1.01 mmol g^{-1}). As a result, only 42% conversion was obtained over 30 wt% TPA/ MgF_2 , which is much lower than that of over $\text{Mg}_{20}\text{F}_{39}\text{TPA-x}$. Thus, the solvothermal solidified $\text{Mg}_{20}\text{F}_{39}\text{TPA-x}$ gives higher density of acidic sites and provides better catalytic performance than that of the immobilized TPA/ MgF_2 .

3.3 Esterification of oleic acid with methanol

Obviously, the most important advantage of single factor is adaptable, and the plans of experiment can be easily updated

based on the result of one test.⁴⁵ In order to get the optimal reaction conditions, single factor design was thus applied to evaluate the effect of methanol/oleic acid molar ratio, catalyst dosage, reaction time and temperature in the esterification of oleic acid, as illustrated in Fig. 5.

3.3.1 The effect of methanol/oleic acid molar ratio. As shown in Fig. 5a, conversion of oleic acid was enhanced from 82% to 95% with the molar ratio of methanol to oleic acid increasing from 6/1 to 9/1. However, the conversion was almost unchanged with the increase of methanol. This phenomenon could be explained by dilution effect, which decreased concentration of catalyst due to excessive methanol.^{46,47}

3.3.2 The effect of catalyst dosage. The conversion lifted slowly with catalyst dosage increased to 5 wt% with methanol/oleic acid molar ratio of 9/1 at 80 °C for 4 h (Fig. 5b). Nevertheless, further increasing the catalyst dosage from 5 wt% to 6 wt% led to a slight decrease of the conversion. It was illustrated that too much catalyst could cause difficult blending of mixture reactants in this reaction system, thus resulting in the reduced performance of the catalyst.⁴⁸

3.3.3 The effect of reaction time. Under the fixed conditions (*i.e.*, 9/1 methanol/oleic acid molar ratio, 80 °C and 4 h), the conversion raised from 68% to 96%, as reaction time increased (Fig. 5c). Despite longer reaction time facilitated the conversion of oleic acid, only 1% conversion was observed after 4–5 h. This phenomenon might be due to the side reactions taking place between products during longer reaction time.⁴⁷ Therefore, the reaction time of 4 h was chosen for subsequent optimization.

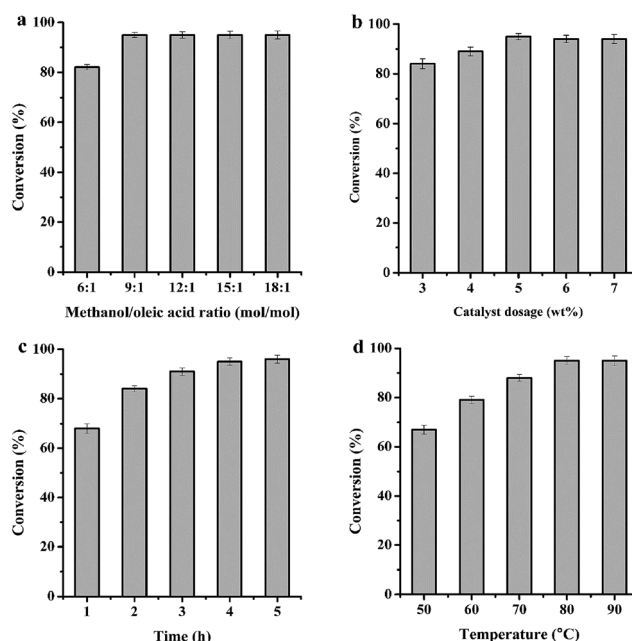


Fig. 5 Conversion of oleic acid over $\text{Mg}_{20}\text{F}_{39}\text{TPA-1.0}$ based on (a) methanol/oleic acid molar ratio = 6/1–18/1, (b) catalyst dosage = 3–7 wt% (catalyst/oleic acid mass ratio), (c) reaction time = 1–5 h, (d) reaction temperature = 50–90 °C. The optimum reaction conditions: methanol/oleic acid molar ratio = 9/1, catalyst dosage = 5 wt%, reaction time = 4 h, reaction temperature = 80 °C.



3.3.4 The effect of reaction temperature. As displayed in Fig. 5d, keeping other conditions same to detect the function of temperature (9/1 molar ratio with 5 wt% catalyst and 4 h). The conversion of oleic acid was significantly improved (69–95%) when reaction temperature was increased from 50 °C to 80 °C, which could be due to the endothermic effect in this reaction system. Yet, excessive heat did not promote the conversion of oleic acid, and it could be found that the conversion stayed largely constant with temperature increasing from 80 °C to 90 °C. It seemed that high temperature exacerbated the methanol vaporization, which was unfavorable to esterification.³⁶

3.4 Leaching experiments

To verify the heterogeneity of catalyst, leaching experiment was carried out. As shown in Fig. S7,† a conversion of 68% was obtained after 1 h at 80 °C. Then $\text{Mg}_{20}\text{F}_{39}\text{TPA-1.0}$ catalyst was filtered and removed from mixtures. The filtrate was continued to react for further 2–5 h without catalyst under the same conditions and the oleic acid conversion remained stable. This result revealed that $\text{Mg}_{20}\text{F}_{39}\text{TPA-1.0}$ was heterogeneous in this reaction system.

3.5 Recyclability of the catalysts

To assess the recyclability feature of $\text{Mg}_{20}\text{F}_{39}\text{TPA-1.0}$ in esterification of oleic acid, the solid catalyst was separated by centrifugation after each recycling test, washed several times with *n*-hexane, dried at 80 °C, and used for the next cycle. To estimate the catalytic ability of $\text{Mg}_{20}\text{F}_{39}\text{TPA-1.0}$ more propitious, about 50% of oleic acid conversion was set for comparison.⁴⁹ As shown in Fig. S8,† The conversion decreased slightly in five consecutive cycles. As demonstrated in Table S1,† residual carbon of 3.70 wt% on used $\text{Mg}_{20}\text{F}_{39}\text{TPA-1.0}$ could be detected by elemental analysis. It could be speculated that the active sites of the catalyst partially covered by organic matter led to the decrease in the conversion.^{50,51} Furthermore, FT-IR and XRD was carried out to fully understand the reasons of catalyst deactivation. Fig. 6 displayed that FT-IR spectra (1200–700 cm^{-1}) of fresh and recycled $\text{Mg}_{20}\text{F}_{39}\text{TPA-1.0}$ catalysts were similar, indicating that Keggin structure remained intact after reused. However, the small peaks were appeared at 2926 cm^{-1} and 2526 cm^{-1} , which were belonged to CH_3 asymmetrical stretching vibrations and CH_2 symmetrical stretching vibrations of methyl oleate, respectively.⁵² As expected, the results of FT-IR and elemental analysis were consistent. The XRD patterns (Fig. 7) of recycled $\text{Mg}_{20}\text{F}_{39}\text{TPA-1.0}$ catalyst (after five recycles) did allow all characteristic diffraction peaks of $\text{Mg}_{20}\text{F}_{39}\text{TPA-1.0}$ to be appeared, although the intensity of diffraction were weak. These results illustrated that $\text{Mg}_{20}\text{F}_{39}\text{TPA-1.0}$ was stable and the decrease of reflection could be due to the adsorption of organic matter.

As shown in Table 4, [BMIM][HSO₄] ionic liquid and sulfonated cation exchange resin (SCER) exhibited good catalytic performance, and oleic acid conversion of 81% and 93% was attained by using the remarkably high catalyst amount of 98 wt% and 47 wt%, respectively (entries 1, 2). Although the phosphorylated carbon (POMC) solid acid catalyst has well-ordered mesoporous structure and large surface area (530 $\text{m}^2 \text{g}^{-1}$), the low

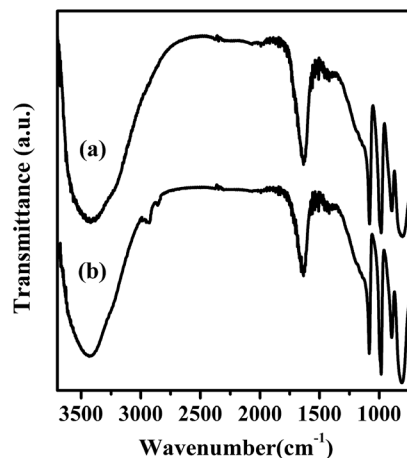


Fig. 6 FT-IR spectra of (a) fresh and (b) reused 5th $\text{Mg}_{20}\text{F}_{39}\text{TPA-1.0}$.

conversion of oleic acid (74%) was obtained (entry 3). In addition, long time and high temperature were typically required to get impressive conversion of oleic acid. For example, 100% conversion could be achieved while prolonging the reaction time to 12 h for $\text{HClSO}_3\text{-ZrO}_2$ (entry 4). WO_3/USY displayed moderate catalytic performance of 74% conversion at 200 °C (entry 5). Even though mesoporous polymeric solid acid (MPD- $\text{SO}_3\text{H-IL}$) possessed high acidity (2.6 mmol g^{-1}) and large surface area (281 $\text{m}^2 \text{g}^{-1}$), good catalytic activity (up to 98% conversion) was achieved when the large molar ratio of methanol and oleic acid (30 : 1) was required (entry 6). Notably, $\text{Mg}_{20}\text{F}_{39}\text{TPA-1.0}$ showed compatible catalytic activity to other heteropoly acid catalysts, but higher temperature (100–120 °C), longer reaction time (7.5 h) and larger molar ratio of methanol and oleic acid (20 : 1) were needed for HPW/H-Y and SWIL/ SiO_2 (entries 7–9). These results clearly demonstrated that the catalytic activity of $\text{Mg}_{20}\text{F}_{39}\text{TPA-1.0}$ presented in this work was more superior to those of previously reported solid acidic catalysts. These results clearly demonstrated that the catalytic activity of $\text{Mg}_{20}\text{F}_{39}\text{TPA-1.0}$ presented in this work was more superior to those of previously reported solid acidic catalysts.

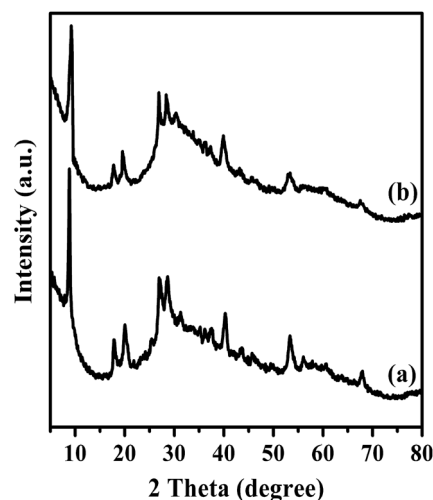


Fig. 7 XRD patterns of (a) fresh and (b) reused 5th $\text{Mg}_{20}\text{F}_{39}\text{TPA-1.0}$.



Table 4 Comparison of esterification of oleic acid over different catalysts

No.	Catalyst	Reaction conditions	Conversion (%)	Ref.
1	[BMIM][HSO ₄]	$T = 87\text{ }^{\circ}\text{C}$, CA = 98 wt%, M/O = 9 : 1, $t = 5\text{ h}$	81	53
2	SCER	$T = 82\text{ }^{\circ}\text{C}$, CA = 47 wt%, M/O = 9 : 1, $t = 8\text{ h}$	93	54
3	POMC	$T = 80\text{ }^{\circ}\text{C}$, CA = 5 wt%, M/O = 15 : 1, $t = 5\text{ h}$	73	55
4	HClSO ₃ -ZrO ₂	$T = 100\text{ }^{\circ}\text{C}$, CA = 3 wt%, M/O = 8 : 1, $t = 12\text{ h}$	100	56
5	WO ₃ /USY	$T = 200\text{ }^{\circ}\text{C}$, CA = 10 wt%, M/O = 6 : 1, $t = 2\text{ h}$	74	57
6	MPD-SO ₃ H-IL	$T = 100\text{ }^{\circ}\text{C}$, CA = 10 wt%, M/O = 30 : 1, $t = 4\text{ h}$	98	14
7	TPA/H-Y	$T = 120\text{ }^{\circ}\text{C}$, CA = 13 wt%, M/O = 20 : 1, $t = 7.5\text{ h}$	98	58
8	SWIL/SiO ₂	$T = 100\text{ }^{\circ}\text{C}$, CA = 5 wt%, M/O = 30 : 1, $t = 4\text{ h}$	97	59
9	Mg ₂₀ F ₃₉ TPA-1.0	$T = 80\text{ }^{\circ}\text{C}$, CA = 5 wt%, M/O = 9 : 1, $t = 4\text{ h}$	95 ± 0.6%	This work

Table 5 Comparison of the catalytic performance of different catalysts in the simultaneous esterification and transesterification

No.	Catalyst	Feedstock	Reaction conditions	Yield (%)	Ref.
1	E-260-20-SO ₃ H	Jatropha oil	$T = 220\text{ }^{\circ}\text{C}$, CA = 5 wt%, M/O = 12 : 1, $t = 5\text{ h}$	93	60
2	Zr-PMOs	Palm oil	$T = 209\text{ }^{\circ}\text{C}$, CA = 13 wt%, M/O = 49 : 1, $t = 6\text{ h}$	85	61
3	FS-B-L-IL	<i>K. integrifoliola</i> oil	$T = 160\text{ }^{\circ}\text{C}$, CA = 10 wt%, M/O = 40 : 1, $t = 10\text{ h}$	93	62
4	Fe ₂ O ₃ -MnO-SO ₄ ²⁻ /ZrO ₂	Waste cooking oil	$T = 180\text{ }^{\circ}\text{C}$, CA = 3 wt%, M/O = 20 : 1, $t = 4\text{ h}$	95	63
5	[BMIm][TS]-ZnCl ₂	Jatropha oil	$T = 200\text{ }^{\circ}\text{C}$, CA = 3 wt%, M/O = 12 : 1, $t = 5\text{ h}$	88	64
6	TPA/Nb ₂ O ₅	Cooking oil	$T = 200\text{ }^{\circ}\text{C}$, CA = 3 wt%, M/O = 18 : 1, $t = 20\text{ h}$	92	65
7	TPA/Al ₂ O ₃	Canola oil	$T = 200\text{ }^{\circ}\text{C}$, CA = 3 wt%, M/O = 6 : 1, $t = 10\text{ h}$	65	66
8	Mg ₂₀ F ₃₉ TPA-1.0	Jatropha oil	$T = 130\text{ }^{\circ}\text{C}$, CA = 8 wt%, M/O = 30 : 1, $t = 12\text{ h}$	93 ± 0.7	This work

3.6 Simultaneous esterification and transesterification of Jatropha oil

Simultaneous esterification and transesterification is highly desired for producing biodiesel from high acid value inedible oil. Thus, Jatropha oil (19.35 mg KOH/g) was selected as feedstock to produce biodiesel over Mg₂₀F₃₉TPA-1.0. The high biodiesel yield 93% was achieved under moderate reaction conditions (methanol/oil molar ratio of 30/1, catalyst dosage of 8 wt%, reaction time of 12 h, reaction temperature of 130 °C), as can be seen in Table S2.† For the simultaneous esterification and transesterification of Jatropha oil, some more sufficient comparison results have been listed in Table 5. It was clear to see that high temperature (160–220 °C) was required to get high biodiesel yield, except for producing biodiesel over Mg₂₀F₃₉TPA-1.0. Especially, higher temperature and longer time were necessary over TPA/Nb₂O₅ and TPA/Al₂O₃ to achieve comparable catalytic activity to Mg₂₀F₃₉TPA-1.0 (entries 6, 7). These results indicated that Mg₂₀F₃₉TPA-1.0 was an excellent catalyst in the simultaneous esterification and transesterification.

As mentioned above, the total acidity of the catalysts played an important role in biodiesel production. Thus, the catalytic performance of the catalysts bearing the same acid density was compared, and the results are shown in Table S3.† The conversion of oleic acid (79 ± 0.9%) and yield of biodiesel (45 ± 1.2%) over Nafion NR50 were higher than those of Amberlyst 15, but relatively higher catalyst amount was needed due to its lower acid density. It was worthy to note that the highest conversion and yield could be obtained over Mg₂₀F₃₉TPA-1.0, which was 95 ± 0.6% and 93 ± 0.7% respectively, possibly due to the stronger acidity resulted from the moiety of heteropoly acids compared with the conventional solid acids.⁶⁷

4. Conclusions

In summary, a range of Mg₂₀F₃₉TPA-*x* hybrids catalysts were prepared by solvothermal method and their catalytic activities were investigated for esterification of oleic acid with methanol. Mg₂₀F₃₉TPA-1.0 was found to exhibit excellent catalytic performance with the conversion of 95% of oleic acid under the optimum esterification reaction conditions (methanol/oleic acid molar ratio of 9 : 1, 5 wt% catalyst dosage at 80 °C for 4 h). Moreover, Mg₂₀F₃₉TPA-1.0 also shows satisfied catalytic activity for the simultaneous esterification and transesterification reaction of high acid value oil, during which 93% yield of biodiesel was achieved at mild conditions. It was found that solvothermal solidified Mg₂₀F₃₉TPA-*x* gives higher density of acidic sites and provides better catalytic performance than that of the immobilized TPA/MgF₂. Further leaching experiment confirms that Mg₂₀F₃₉TPA-1.0 was heterogeneous in this reaction system. And the catalyst still keeps high catalytic activity after five consecutive cycles. Therefore, the Mg₂₀F₃₉TPA-1.0 catalyst described herein shows great potential for biodiesel production.

Acknowledgements

We gratefully acknowledge the National Natural Science Foundation of China (21576059, 21666008), the Key Technologies R&D Program (2014BAD23B01), and the Innovation Fund for Graduate Students of Guizhou University (No. 2016075).

References

- 1 C. Z. Liu, F. Wang, A. R. Stiles and C. Guo, *Appl. Energy*, 2012, **92**, 406.



- 2 W. Liu, P. Yin, X. G. Liu, S. H. Zhang and R. J. Qu, *J. Ind. Eng. Chem.*, 2015, **21**, 893.
- 3 Y. Chang, C. Lee and C. Bae, *RSC Adv.*, 2014, **4**, 47448.
- 4 R. Luque, J. C. Lovett, B. Datta, J. Clancy, J. M. Campelo and A. A. Romero, *Energy Environ. Sci.*, 2010, **3**, 1706.
- 5 S. Sankaranarayanan, C. A. Antonyraj and S. Kannan, *Bioresour. Technol.*, 2012, **109**, 57.
- 6 I. K. Hong, H. Jeon, H. Kim and S. B. Lee, *J. Ind. Eng. Chem.*, 2016, **42**, 107.
- 7 J. A. Melero, J. Iglesias and G. Morales, *Green Chem.*, 2009, **11**, 1285.
- 8 A. F. Lee, J. A. Bennett, J. C. Manayil and K. Wilson, *Chem. Soc. Rev.*, 2014, **43**, 7887.
- 9 L. J. Konwar, J. Boro and D. Deka, *Renewable Sustainable Energy Rev.*, 2014, **29**, 546.
- 10 D. Meloni, D. Perra, R. Monaci, M. G. Cutrufello, E. Rombi and I. Ferino, *Appl. Catal., B*, 2016, **184**, 163.
- 11 Q. Zhou, H. Zhang, F. Chang, H. Li, H. Pan, W. Xue, D. Y. Hu and S. Yang, *J. Ind. Eng. Chem.*, 2015, **31**, 385.
- 12 X. Deng, Z. Fang and Y. H. Liu, *Energy Convers. Manage.*, 2010, **51**, 2802.
- 13 S. Jansri, S. B. Ratanawilai, M. L. Allen and G. Prateepchaikul, *Fuel Process. Technol.*, 2011, **92**, 1543.
- 14 H. Pan, H. Li, X. F. Liu, H. Zhang, K. L. Yang, S. Huang and S. Yang, *Fuel Process. Technol.*, 2016, **150**, 50.
- 15 H. Amani, Z. Ahmad, M. Asif and B. H. Hameed, *J. Ind. Eng. Chem.*, 2014, **20**, 4437.
- 16 D. A. G. Aranda, R. T. P. Santos, N. C. O. Tapanes, A. L. D. Ramos and O. A. C. Antunes, *Catal. Lett.*, 2008, **122**, 20.
- 17 K. Y. Nandiwale and V. V. Bokade, *Ind. Eng. Chem. Res.*, 2014, **53**, 18690.
- 18 R. M. N. Kalla, M. R. Kim, Y. N. Kim and L. Kim, *New J. Chem.*, 2016, **40**, 687.
- 19 D. Y. Zhang, M. H. Duan, X. H. Yao and Y. J. Fu, *Fuel*, 2016, **172**, 293.
- 20 Z. W. Wu, C. Chen, Q. R. Guo, B. X. Li, Y. G. Que, L. Wang, H. Wan and G. F. Guan, *Fuel*, 2016, **184**, 128.
- 21 K. Saravanan, B. Tyagi and H. C. Bajaj, *Appl. Catal., B*, 2016, **192**, 161.
- 22 S. Y. Chen, S. Lao-ubol, T. Mochizuki, Y. Abe, M. Toba and Y. Yoshimura, *Bioresour. Technol.*, 2014, **157**, 346.
- 23 K. Malins, J. Brinks, V. Kampars and I. Malina, *Appl. Catal., A*, 2016, **519**, 99.
- 24 I. V. Kozhevnikov, *Chem. Rev.*, 1998, **98**, 171.
- 25 T. Okuhara, N. Mizuno and M. Misono, *Adv. Catal.*, 1996, **41**, 113.
- 26 T. Okuhara, T. Nishimura and M. Misono, *Stud. Surf. Sci. Catal.*, 1996, **101**, 581.
- 27 M. Misono, *Chem. Commun.*, 2001, **13**, 1141.
- 28 J. Li, X. H. Wang, W. M. Zhu and F. H. Cao, *ChemSusChem*, 2009, **2**, 177.
- 29 J. A. Monge, G. Trautwein and J. P. M. Lozar, *Appl. Catal., A*, 2013, **468**, 432.
- 30 C. F. Oliveira, L. M. Dezaneti, F. A. C. Garcia, J. L. Macedo, J. A. Dias, S. C. L. Dias and K. S. P. Alvim, *Appl. Catal., A*, 2010, **372**, 153.
- 31 J. W. Sun, P. F. Yan, G. H. An, J. Q. Sha, G. M. Li and G. Y. Yang, *Sci. Rep.*, 2016, **6**, 25595.
- 32 Z. Bian, S. Zhang, X. Zhu, Y. Li, H. Liu and J. Hu, *RSC Adv.*, 2015, **5**, 31502.
- 33 J. Li, D. F. Li, J. Y. Xie, Y. Q. Liu, Z. J. Guo, Q. Wang, Y. Lyu, Y. Zhou and J. Wang, *J. Catal.*, 2016, **339**, 123.
- 34 S. H. Zhu, X. Q. Gao, F. Dong, Y. L. Zhu, H. Y. Zheng and Y. W. Li, *J. Catal.*, 2013, **306**, 155.
- 35 S. Wuttke, S. M. Coman, G. Scholz, H. Kirmse, A. Vimont, M. Daturi, S. L. M. Schroeder and E. Kemnitz, *Chem.–Eur. J.*, 2008, **14**, 11488.
- 36 F. Zhang, Z. Fang and Y. T. Wang, *Appl. Energy*, 2015, **155**, 637.
- 37 K. Jagadeeswaraiyah, C. R. Kumar, P. S. S. Prasad and N. Lingaiah, *Catal. Sci. Technol.*, 2014, **4**, 2969.
- 38 M. X. Cheng, T. Shi, H. Y. Guan, S. T. Wang, X. H. Wang and Z. J. Jiang, *Appl. Catal., B*, 2011, **107**, 104.
- 39 L. Y. Meng, S. R. Zhai, Z. C. Sun, F. Zhang, Z. Y. Xiao and Q. D. An, *Microporous Mesoporous Mater.*, 2015, **204**, 123.
- 40 Z. Zillillah, T. A. Ngu and Z. Li, *Green Chem.*, 2014, **16**, 1202.
- 41 F. Richard, S. Célrier, M. Vilette, J. D. Comparot and V. Montouillout, *Appl. Catal., B*, 2014, **152–153**, 241.
- 42 I. A. Telleria, Y. Guo, F. Hemmann, P. L. Arias and E. Kemnitz, *Catal. Sci. Technol.*, 2014, **4**, 1357.
- 43 X. Mo, D. E. López, K. Suwannakarn, Y. Liu, E. Lotero, J. G. Goodwin and C. Lu, *J. Catal.*, 2008, **254**, 332.
- 44 X. X. Han, H. Du, C. T. Hung, L. L. Liu, P. H. Wu, D. H. Ren, S. J. Huang and S. B. Liu, *Green Chem.*, 2015, **17**, 499.
- 45 N. Sudarsanam and D. Frey, *Qual. Reliab. Eng. Int.*, 2011, **27**, 947.
- 46 Y. Zhang, W. T. Wong and K. F. Yung, *Appl. Energy*, 2014, **116**, 191.
- 47 X. X. Han, K. K. Chen, W. Yan, C. T. Hung, L. L. Liu, P. H. Wu, K. C. Lin and S. B. Liu, *Fuel*, 2016, **165**, 115.
- 48 F. Zhang, Z. Fang and Y. T. Wang, *Appl. Energy*, 2015, **155**, 637.
- 49 H. Li, Z. Fang, J. Luo and S. Yang, *Appl. Catal., B*, 2017, **200**, 182.
- 50 H. Li, S. Saravanamurugan, S. Yang and A. Riisager, *Green Chem.*, 2016, **18**, 726.
- 51 J. He, H. Li, Y. X. Liu, W. F. Zhao, T. T. Yang, W. Xue and S. Yang, *J. Ind. Eng. Chem.*, 2016, **43**, 133.
- 52 J. Erkelens and T. J. Liefkens, *J. Catal.*, 1966, **5**, 542.
- 53 A. H. M. Fauzi and N. Amin, *Energy Convers. Manage.*, 2013, **76**, 818.
- 54 Y. Jiang, J. Lu, K. Sun, L. Ma and J. Ding, *Energy Convers. Manage.*, 2013, **76**, 980.
- 55 L. Wang, X. Dong, H. Jiang, G. Li and M. Zhang, *Catal. Commun.*, 2014, **56**, 164.
- 56 Y. Zhang, W. Wong and K. Yung, *Appl. Energy*, 2014, **116**, 191.
- 57 A. Costa, P. Braga, J. de Macedo, J. Dias and S. Dias, *Microporous Mesoporous Mater.*, 2014, **147**, 142.
- 58 C. Baroi and A. K. Dalai, *Appl. Catal., A*, 2014, **485**, 99.
- 59 B. Zhen, H. Li, Q. Jiao, Y. Li, Q. Wu and Y. Zhang, *Ind. Eng. Chem. Res.*, 2012, **51**, 10374.
- 60 M. Huang, J. Luo, Z. Fang and H. Li, *Appl. Catal., B*, 2016, **190**, 103.



- 61 R. Sánchez-Vázquez, C. Pirez, J. Iglesias, K. Wilson, A. F. Lee and J. A. Melero, *ChemCatChem*, 2013, **5**, 994.
- 62 H. Zhang, H. Li, H. Pan, X. Liu, K. Yang, S. Huang and S. Yang, *Energy Convers. Manage.*, 2017, **138**, 45.
- 63 F. Alhassan, U. Rashid and Y. Taufiq-Yap, *Fuel*, 2015, **142**, 38.
- 64 F. Guo, Z. Fang, X. Tian, Y. Long and L. Jiang, *Bioresour. Technol.*, 2013, **140**, 447.
- 65 V. Brahmkhatri and A. Patel, *Fuel*, 2012, **102**, 72.
- 66 K. Narasimharao, D. R. Brown, A. F. Lee, A. D. Newman, P. F. Siril, S. J. Tavener and K. Wilson, *J. Catal.*, 2007, **248**, 226.
- 67 N. Narkhede, S. Singh and A. Patel, *Green Chem.*, 2015, **17**, 89.

